

p53 Loss in MYC-Driven Neuroblastoma Leads to Metabolic Adaptations Supporting Radioresistance

Orli Yogev¹, Karen Barker¹, Arti Sikka², Gilberto S. Almeida^{1,3}, Albert Hallsworth¹, Laura M. Smith¹, Yann Jamin³, Ruth Ruddle⁴, Alexander Koers¹, Hannah T. Webber¹, Florence I. Raynaud⁴, Sergey Popov^{4,5}, Chris Jones^{4,5}, Kevin Petrie¹, Simon P. Robinson³, Hector C. Keun², and Louis Chesler¹

Abstract

Neuroblastoma is the most common childhood extracranial solid tumor. In high-risk cases, many of which are characterized by amplification of *MYCN*, outcome remains poor. Mutations in the p53 (*TP53*) tumor suppressor are rare at diagnosis, but evidence suggests that p53 function is often impaired in relapsed, treatment-resistant disease. To address the role of p53 loss of function in the development and pathogenesis of high-risk neuroblastoma, we generated a *MYCN*-driven genetically engineered mouse model in which the tamoxifen-inducible p53ER^{TAM} fusion protein was expressed from a knock-in allele (Th-*MYCN/Trp53*^{KI}). We observed no significant differences in tumor-free survival between Th-*MYCN* mice heterozygous for *Trp53*^{KI} ($n = 188$) and Th-*MYCN* mice with wild-type p53 ($n = 101$). Conversely, the survival of Th-*MYCN/Trp53*^{KI/KI} mice lacking functional p53 ($n = 60$) was greatly reduced. We found that Th-*MYCN/Trp53*^{KI/KI} tumors were resistant to ionizing

radiation (IR), as expected. However, restoration of functional p53ER^{TAM} reinstated sensitivity to IR in only 50% of Th-*MYCN/Trp53*^{KI/KI} tumors, indicating the acquisition of additional resistance mechanisms. Gene expression and metabolic analyses indicated that the principal acquired mechanism of resistance to IR in the absence of functional p53 was metabolic adaptation in response to chronic oxidative stress. Tumors exhibited increased antioxidant metabolites and upregulation of glutathione S-transferase pathway genes, including *Gstp1* and *Gstz1*, which are associated with poor outcome in human neuroblastoma. Accordingly, glutathione depletion by buthionine sulfoximine together with restoration of p53 activity resensitized tumors to IR. Our findings highlight the complex pathways operating in relapsed neuroblastomas and the need for combination therapies that target the diverse resistance mechanisms at play. *Cancer Res*; 76(10); 3025–35. ©2016 AACR.

Introduction

p53 is a critical tumor suppressor that performs a diverse range of functions, including induction of apoptosis, senescence, and DNA repair in response to genotoxic stress. Deregulation of its activity is associated with tumor initiation and progression as well as resistance to therapy. Recent *in vivo* evidence indicates that the role of p53 as a tumor suppressor is independent of its canonical role as a cell cycle, senescence, and proapoptosis regulator, and

may be due to other p53-dependent activities such as maintenance of DNA stability and metabolic adaptation (1). In the last decade, a role for p53 in metabolic adaptation has been identified (2, 3), often activated by metabolic stress induced by low oxygen levels or nutrient scarcity (3). This leads to changes in several metabolic mechanisms affecting energy homeostasis, such as glycolysis, downregulation of reactive oxygen species (ROS), oxidative phosphorylation (OXPHOS), β -oxidation, and gluconeogenesis (4). However, to date, there is no direct evidence demonstrating an advantage in tumor survival or growth *in vivo* due to metabolic alterations induced by p53 loss of function.

Neuroblastoma is the most common extracranial pediatric solid tumor, and amplification of the *MYCN* gene is a predictor of high-risk disease. Treatment options for high-risk patients include intensive cytotoxic chemotherapy and surgical resection, myeloablative autologous stem cell transplantation, radiotherapy, and intensive multimodal therapy. Although most high-risk patients initially respond to therapy, a majority of these patients will relapse with treatment-resistant disease. Approximately 50% of relapsed tumors are associated with p53 loss of function, mainly through alterations to the p53 pathway. In contrast with other MYC-driven cancers, such as medulloblastoma (5) and lymphoma, mutation of genes in the p53 pathway is rare at diagnosis (6), implying that selection for p53 pathway deficiency occurs following treatment. Additional mechanisms such as epigenetic alterations and metabolic adaptation have also been

¹Division of Clinical Studies, The Institute of Cancer Research, London, United Kingdom. ²Department of Surgery and Cancer, Imperial College, London, United Kingdom. ³Division of Radiotherapy and Imaging, The Institute of Cancer Research, London, United Kingdom. ⁴Division of Cancer Therapeutics, The Institute of Cancer Research, London, United Kingdom. ⁵Department of Molecular Pathology, The Institute of Cancer Research, London, United Kingdom.

Note: Supplementary data for this article are available at Cancer Research Online (<http://cancerres.aacrjournals.org/>).

Current address for K. Petrie: School of Natural Sciences, University of Stirling, Stirling, United Kingdom.

Corresponding Author: Louis Chesler, The Institute of Cancer Research, 15 Cotswold Road, Sutton, Surrey SM2 5NG, United Kingdom. Phone: 02087224176; E-mail: louis.chesler@icr.ac.uk

doi: 10.1158/0008-5472.CAN-15-1939

©2016 American Association for Cancer Research.

implicated in aggressive neuroblastoma (7–11). To better understand the role of p53 in the development of high-risk therapy-resistant neuroblastoma, we generated a MYCN-driven genetically engineered mouse (GEM) model with inducible p53 loss of function.

Materials and Methods

In vivo studies

All experimental protocols were monitored and approved by The Institute of Cancer Research Animal Welfare and Ethical Review Body, in compliance with the UK Home Office Animals (Scientific Procedures) Act 1986, the United Kingdom National Cancer Research Institute guidelines for the welfare of animals in cancer research (12), and the ARRIVE (Animal Research: Reporting of In Vivo Experiments) guidelines (13). Th-MYCN mice (129×1/SvJ-Tg(Th-MYCN)41Waw/Nci) have been described previously (14). The Trp53^{KI/KI} mice were kindly provided by G.I. Evan (15) and crossed with Th-MYCN animals into a background of the 129×1/SvJ-Tg(Th-MYCN)41Waw/Nci (for more than 15 generations). Transgenic Th-MYCN/Trp53^{KI} animals with palpable tumor were allocated to treatment or control groups. Restoration of wild-type (WT) p53 was achieved by administration of chow-containing tamoxifen at 400 mg/kg to provide a daily dose of approximately 64 mg/kg. Animals were monitored twice a week by palpation for detectable tumors (>5 mm) and were sacrificed upon detection of a tumor larger than 15 mm diameter. Mice were allowed access to sterilized food and water *ad libitum*.

In vivo imaging

Multi-slice ¹H MRI was performed on a 7T horizontal bore microimaging system (Bruker Instruments) using a 3-cm birdcage coil. Anesthesia was induced using a gaseous mixture of 2% isoflurane/oxygen (v/v). Core body temperature was maintained by warm air blown through the magnet bore. T₂-weighted coronal and transverse images were acquired from 20 contiguous 1-mm-thick slices through the mouse abdomen, using a rapid acquisition with refocused echoes (RARE) sequence with 4 averages of 128 phase encoding steps over a 3 × 3 cm field of view, an echo time (TE) of 36 ms, a repetition time (TR) of 4.5 seconds, and a RARE factor of 8. The resolution was 0.234 × 0.234 mm/pixel, and the acquisition time was 3 minutes 24 seconds. Volumetric data were analyzed using in-house software (ImageView; ref. 16).

Immunoblot analysis

Total protein was extracted from equal size tumor pieces in SDS sample buffer using Precellys24. The following antibodies were used to detect protein levels (all from Cell Signaling Technology): phospho-p53 (9284), cleaved caspase-3 (CC3) (9661), caspase-3 (9665), p-ATM (5883), phospho-ATR (2853), phospho-CHK2 (2661), GAPDH (8884), γ-H2AX (9718), and tubulin (2128). Also used were antibodies against p19ARF (Novus Biologicals; 5-c3-1) and horseradish peroxidase (HRP)-conjugated-p53 (R&D System; HAF1355). Proteins were detected using HRP-conjugated anti-mouse and anti-rabbit antibodies (Dako), ECL Ultra (TMA-6; Lumigen) and imaged using a Fujifilm LAS-4000 system.

Immunohistochemistry

Tumors were processed using a ASP300S tissue processor (Leica) according to the manufacturer's instructions. Sections

were deparaffinized and rehydrated through Histo-Clear and graded alcohol series, rinsed for 5 minutes in tap water, boiled for 5 minutes in 1% citric buffer, and left to cool to room temperature. Endogenous enzyme activity was blocked by 1% H₂O₂ for 20 minutes followed by three washes in ddH₂O. For mouse antibodies, we used the M.O.M kit (Vector BMK-2202), for rabbit, the following protocol was used: blocking for >1 hour in PBS 0.01% Triton, 5% BSA, 1st antibody was incubated at room temperature overnight 1:100 to 1:500, washed in TBS, 2nd Biotinylated Anti Rabbit was incubated at room temperature for >2 hours (1:500), 3rd avidin HRP-conjugated (A2664; 1:1,000) 1 hour at room temperature. Antibody solution: PBS 0.01% Triton and 1% BSA. Sections were stained for 1 to 5 minutes using Vector Imm PACT DAB (SK-4105). We used the following antibodies: CD31 (ab28364), CC3 (Cell Signaling Technology; 9661), neurofilament-L (NF-L; Cell Signaling Technology; 2837), and Tuj-1 (R&D Systems; BAM1195). Sections were counterstained with hematoxylin and eosin (H&E). Immunofluorescence staining was performed using Invitrogen Alexa Fluor 488 goat anti-rabbit. Images were captured by confocal microscopy (LSM700, LSM T-PMT) and processed by ZEN2012 (Zeiss) software.

Real-time PCR

Total RNA was isolated from tumor tissue using the miRNAeasy mini Kit (Qiagen) and cDNA prepared using Superscript II Reverse Transcriptase (Life Technologies). Quantitative PCR was performed in triplicate using Taqman Gene Expression Mix (Life Technologies) and gene-specific primers for *Cdkn1a* (Mm04205640), *Puma* (Mm00519268), *Noxa-1* (Mm00549172), *Bax* (Mm00432051), and *Actb* (Mm00607939; Life Technologies). Relative expression was calculated according to the ΔΔCt relative quantification method against the average expression of control tumors.

Hypoxia

Tumor hypoxia was assessed as previously described (16, 17). Briefly, tumor-bearing mice received 60 mg/kg i.p. of the hypoxia marker pimonidazole hydrochloride (Hypoxyprobe). After 45 minutes, tumors were rapidly excised, snap-frozen, and stored in liquid nitrogen. Sections were either stained using Hypoxyprobe-1 plus FITC-conjugated mouse monoclonal antibodies (1:100) or HRP-conjugated rabbit anti-FITC (Hypoxyprobe-1 Plus Kit).

Quantitation of ROS

Freshly excised tumor samples (~20 mg) were incubated with 10 μmol/L CellROX Oxidative Stress (Molecular probes; C10444) for 1 hour. Subsequently, single cells were washed twice with PBS and fixed with 4% PFA for 1 hour, washed in PBS, and acquired by FACS (BD-LSRII) using FACSDiva software (BD Biosciences). Sample were analyzed by FlowJo (FlowJo LLC).

Glutathione assay

Glutathione was measured in fresh tumor samples using the GSH-Glo glutathione assay (Promega). Luciferase levels were normalized to tissue mass.

Statistical analysis

Samples were compared using one-way ANOVA or two-way ANOVA as indicated and *post-hoc* Bonferroni multiple comparison tests using GraphPad Prism; *P* values < 0.05 were considered as statistically significant.

Results

Th-MYC*N* transgenic mice display a normal p53 response

During tumorigenesis, the expression or activity of checkpoint regulators, including p53, is often suppressed. We sought to establish whether this is also the case in our GEM model of MYC*N*-driven neuroblastoma (Th-MYC*N*). To this end, we tested the levels of the p53 upstream regulator p19^{Arf} in matched tumor and spleen tissues and found similar protein expression levels (Supplementary Fig. S1A), suggesting that the p53 pathway is intact. We also examined p53 activation following stress by exposing Th-MYC*N* tumor-bearing mice to 5 Gy ionizing radiation (IR). The p53 pathway was induced by IR as evidenced by increased levels of transcriptionally active p53 phosphorylated at serine 15 (p-p53^{Ser15}) in tumors, spleen, and thymus (Supplementary Fig. S1B), as well as an increase in the p53 target gene *Cdkn1a* (p21^{Cip1/Waf1}; Supplementary Fig. S1C). Furthermore, we found tumor-specific upregulation of the proapoptotic gene *Bbc3* (*Puma*), but not the proapoptotic genes *Pmaip1* (*Noxa*) or *Bax* (Supplementary Fig. S1C and S1D). Both the cyclin-dependent kinase inhibitor p21 and PUMA are well-characterized effectors of p53-mediated growth arrest and apoptosis. Consistent with this, apoptosis was enhanced as evidenced by the presence of CC3 in the tumor and the thymus (Supplementary Figs. S1B and S2). Induction of DNA damage was demonstrated by the presence of phosphorylated histone gamma-H2AX (γ -H2AX), primarily in the spleen and the gut (Supplementary Fig. S2). Taken together, these results suggest that Th-MYC*N* mice are representative of p53 WT human neuroblastoma.

p53 loss of function leads to increased tumor penetrance in Th-MYC*N* hemizygous mice

In order to evaluate p53 loss of function in neuroblastoma, we crossed Th-MYC*N* mice (in which expression of a human MYC*N* transgene is directed by a rat tyrosine hydroxylase (Th) promoter to neural crest cells during early development; ref. 14) with a GEM model conditionally deficient for functional p53 (Fig. 1A; ref. 15). Here, the endogenous *Trp53* gene is replaced with a knock-in allele (*Trp53*^{KI}) encoding a 4-hydroxytamoxifen (4-OHT)-regulatable p53ER^{TAM} fusion protein. In the presence of 4-OHT (a metabolite of tamoxifen, Tam), the hormone-binding domain of the estrogen receptor (ER) is released from its inhibitory conformation, and p53ER^{TAM} is translocated to the nucleus. Homozygous Th-MYC*N* transgenic mice display 100% penetrance (18), developing tumors within 7 to 8 weeks of birth, whereas only 16% of hemizygous Th-MYC*N* transgenic mice with WT *Trp53* (Th-MYC*N*/*Trp53*^{WT/WT}) developed tumors by 21 weeks of age with a median latency of 62 days (Fig. 1B; Supplementary Table S1). Thus, penetrance and latency in the Th-MYC*N* GEM model are dependent on transgene dosage, and in this study, only heterozygous Th-MYC*N* mice were used. While Th-MYC*N* mice heterozygous for MYC*N* and *Trp53*^{KI} (Th-MYC*N*/*Trp53*^{KI/WT}) displayed a moderate increase in penetrance to 27% with no significant decrease in tumor-free survival, this increased dramatically to 75% for mice homozygous for *Trp53*^{KI} (Th-MYC*N*/*Trp53*^{KI/KI}). No littermates lacking Th-MYC*N*, either heterozygous or homozygous for *Trp53*^{KI}, developed neuroblastomas by 200 days. While *Trp53*^{KI} homozygosity increased penetrance, this had no effect on either latency or tumor growth rate as measured by volumetric MRI (Fig. 1C).

To test whether the increased tumor incidence in Th-MYC*N*/*Trp53*^{KI/WT} mice was due to a mutation in the WT *Trp53* allele, we

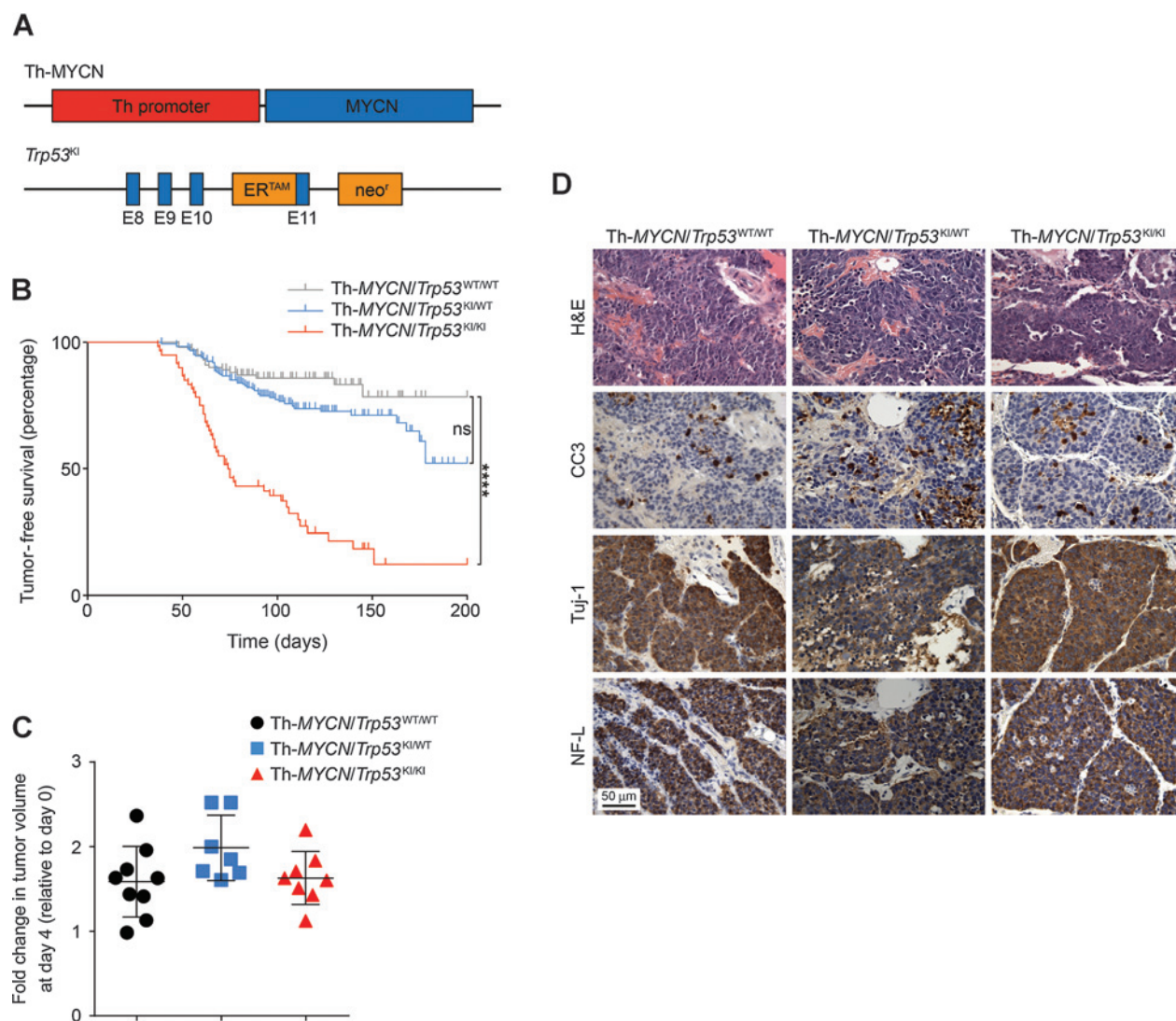
sequenced exons 5 to 9 (corresponding to the p53 DNA-binding domain) in Th-MYC*N*/*Trp53*^{WT/WT} ($n = 16$), Th-MYC*N*/*Trp53*^{KI/WT} ($n = 12$), and Th-MYC*N*/*Trp53*^{KI/KI} ($n = 11$) tumors. We found only one mutation arising in the Th-MYC*N*/*Trp53*^{KI/WT} cohort (Supplementary Table S2), supporting the notion that increased tumor penetrance in Th-MYC*N*/*Trp53*^{KI/WT} mice is not caused by inactivation of the remaining WT *Trp53* allele. We also examined whether postnatal Tam-induced restoration of functional p53 could affect tumor penetrance, latency, and growth rate. We administered Tam to tumor-bearing mice aged 50 to 80 days as well as to 30-day old mice, a timepoint at which tumors are not yet detectable. We found that restoration of functional p53ER^{TAM} had no effect on tumor growth rate or penetrance in Th-MYC*N*/*Trp53*^{KI/KI} mice (Supplementary Fig. S3A and S3B).

Pathologic investigations in Th-MYC*N*/*Trp53*^{KI} transgenic mice revealed that they developed paravertebral, thoracic, or abdominal solid tumors, consistent with a parasympathetic origin in common with the Th-MYC*N* GEM model. Immunohistochemical analysis revealed that all Th-MYC*N*/*Trp53*^{KI} tumors stained positive for the neuroblastoma markers Tuj-1 and NF-L (Fig. 1D). Furthermore, in agreement with the parasympathetic origin of the Th-MYC*N* tumors (19), histopathologic analysis revealed an increase in the percentage of pups positive for neuroblast hyperplasia in the Th-MYC*N*/*Trp53*^{KI/KI} compared with Th-MYC*N*/*Trp53*^{WT/WT} (Supplementary Fig. S4). Thus, our results suggested that p53 loss of function interacts with aberrant expression of MYC*N* at an early stage of neuroblastoma tumorigenesis. However, p53 deficiency did not affect latency or tumor growth rate.

MYC*N*-driven neuroblastomas deficient for p53 are resistant to apoptosis induced by IR

Given that p53 pathway alterations are associated with relapsed/treatment-resistant neuroblastoma, we tested whether p53 deficiency conferred an antiapoptotic advantage to tumors in Th-MYC*N*/*Trp53*^{KI/KI} mice. External beam radiotherapy is widely used in neuroblastoma treatment following induction chemotherapy and surgery, although a period of remission is often followed by subsequent relapse in high-risk cases (20). To examine a role for p53 deficiency in treatment-resistant neuroblastoma, we exposed Th-MYC*N*/*Trp53*^{WT/WT} and Th-MYC*N*/*Trp53*^{KI/KI} tumor-bearing mice to IR in the presence or absence of tamoxifen. In Th-MYC*N*/*Trp53*^{WT/WT} tumors, 5 Gy IR induced apoptosis 5.5 hours after IR as measured by the presence of pyknotic nuclei in 90% to 95% of the cells (Fig. 2A). By contrast, Th-MYC*N*/*Trp53*^{KI/KI} tumors were found to be resistant to IR-induced apoptosis. This resistance was maintained in some individual animals upon Tam-induced restoration of functional p53ER^{TAM} with responses ranging from IR resistance to complete response (Fig. 2A). IR also failed to significantly improve survival in Th-MYC*N*/*Trp53*^{KI/KI} allografts, providing evidence for intrinsic resistance to IR in these tumors (Fig. 2B). While the degree of activation of p53ER^{TAM} was similar (as measured by nuclear p-p53^{Ser15} and induction of *Cdkn1a* expression) after IR and Tam administration, this did not correlate with induction of apoptosis. Furthermore, tumors that showed a similar degree of p53 activation displayed differences in apoptotic response (Fig. 2C and D). Pharmacokinetic analysis (LC-MS/MS) of Tam levels supported these findings with results showing a significant correlation between levels of Tam and 4-OHT but no apoptotic response (Fig. 2E). Collectively, these results suggest that p53 loss of function confers an antiapoptotic advantage to tumors in response to cytotoxic IR, and that a

Yogev et al.

**Figure 1.**

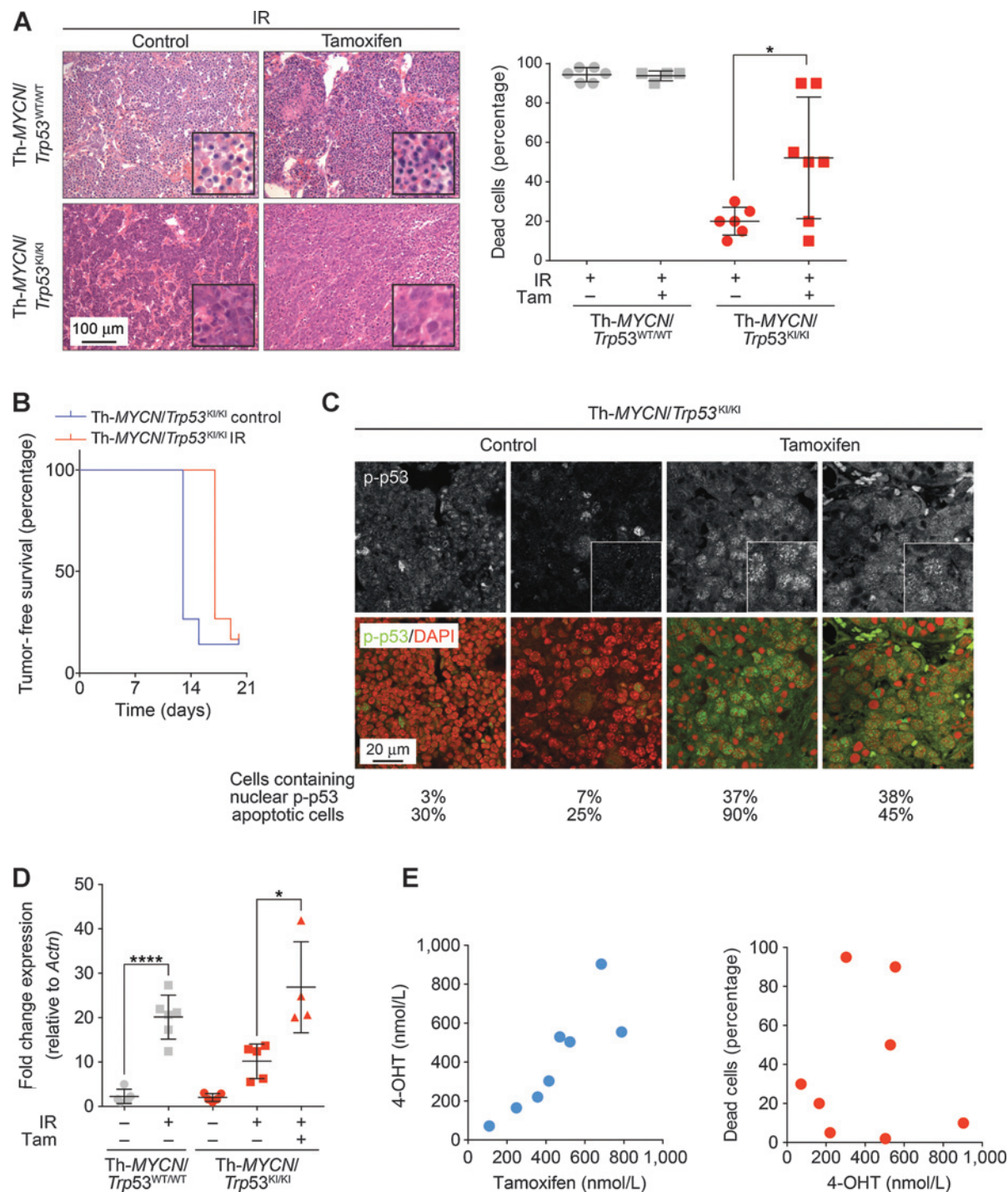
p53 deficiency leads to increased tumor penetrance in MYCN-driven neuroblastoma. A, Th-MYCNI transgenic mice were crossed with a GEM model comprising a knock-in of the *Trp53* allele (*Trp53*^{KI}) expressing tamoxifen-regulatable p53ER^{TAM}. B, Kaplan-Meier survival curves for Th-MYCNI/Trp53^{WT/WT} (*n* = 101), Th-MYCNI/Trp53^{KI/WT} (*n* = 188; ns, nonsignificant, *P* = 0.06), or Th-MYCNI/Trp53^{KI/KI} (*n* = 60; ****, *P* < 0.0001) transgenic mice as indicated. Log-rank test. C, tumor volume change (relative to day 0) determined by MRI at day 4 for Th-MYCNI/Trp53^{WT/WT} (*n* = 9), Th-MYCNI/Trp53^{KI/WT} (*n* = 7), and Th-MYCNI/Trp53^{KI/KI} mice (*n* = 8). D, representative images of tumor sections from Th-MYCNI/Trp53^{WT/WT}, Th-MYCNI/Trp53^{KI/WT}, and Th-MYCNI/Trp53^{KI/KI} tumors subjected to H&E and immunohistochemical staining for the marker of apoptosis CC3, and neuroblastoma markers Tuj1 and NF-L (brown). Cell nuclei were counterstained with hematoxylin. Scale bar, 50 μm.

fraction of Th-MYCNI/Trp53^{KI/KI} tumors develop resistance to restoration of p53 function.

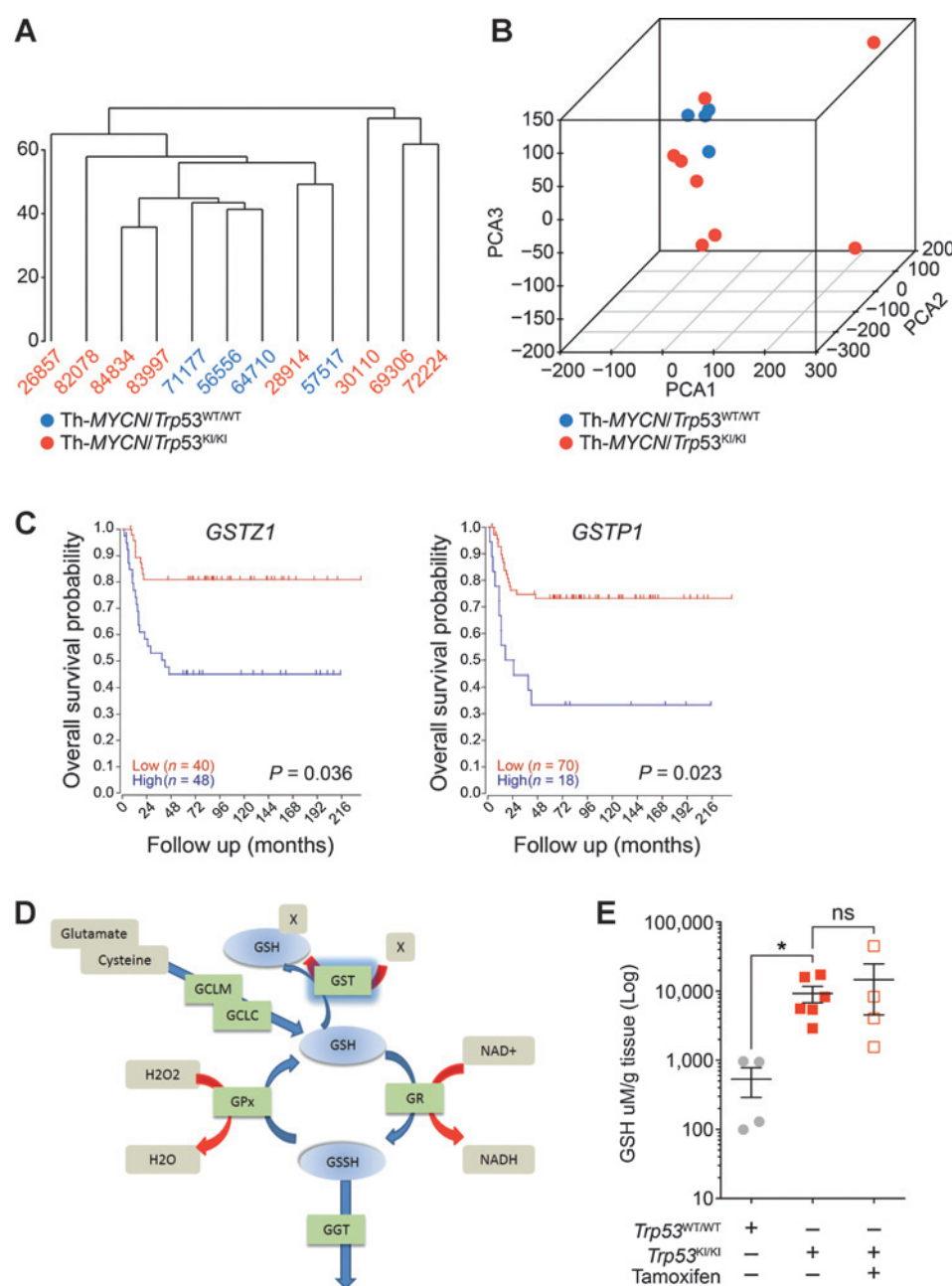
p53 loss of function leads to upregulation of the GSH antioxidant metabolic pathway in MYCN-driven neuroblastoma

To characterize the mechanisms underlying resistance to IR in Th-MYCNI/Trp53^{KI/KI} tumors, we performed Affymetrix expression microarray analysis. Surprisingly, few genes (only 38 protein-coding transcripts) were altered across the Th-MYCNI/Trp53^{KI/KI} cohort of tumor samples compared with Th-MYCNI/Trp53^{WT/WT} tumors. This may be due to a high

degree of intertumoral heterogeneity in the pattern of gene expression among Th-MYCNI/Trp53^{KI/KI} tumors as revealed by hierarchical clustering (Fig. 3A) and principal component analysis (Fig. 3B). While Th-MYCNI/Trp53^{WT/WT} tumors cluster together tightly, this is not replicated in the Th-MYCNI/Trp53^{KI/KI} cohort. Thus, to identify pathways that may be altered in common among Th-MYCNI/Trp53^{KI/KI} tumors, we analyzed gene expression in individual Th-MYCNI/Trp53^{KI/KI} tumors against the Th-MYCNI/Trp53^{WT/WT} control cohort. Differentially expressed genes were combined, and analysis of the composite gene list revealed seven significantly altered pathways between the groups (Supplementary Table S3). Of these,

**Figure 2.**

Tumors deficient for p53 exhibit p53-dependent and -independent treatment resistance. A, mice bearing 5 mm palpable tumors were placed on normal or tamoxifen diet for 5 days followed by whole-body irradiation (IR, 5 Gy) or mock treatment. Irradiated Th-MYCNI/Trp53^{WT/WT} tumors treated ($n = 6$) or untreated ($n = 4$) with tamoxifen and irradiated Th-MYCNI/Trp53^{KI/KI} tumors treated ($n = 6$) or untreated ($n = 7$) with tamoxifen were analyzed to quantify dead cells as indicated by H&E (left) and percentage values (right). Scale bar, 100 μ m. *, $P = 0.03$, unpaired t test. B, tumor-free survival analysis of Th-MYCNI/Trp53^{KI/KI} allografts from primary tissue, control ($n = 8$), and irradiated ($n = 8$). C, immunofluorescence analysis of phosphorylated p53 (p-p53) of Th-MYCNI/Trp53^{KI/KI} irradiated Th-MYCNI/Trp53^{KI/KI} tumors treated ($n = 6$) or untreated ($n = 7$) with tamoxifen. Bottom plot shows cells stained with p-p53 (green) counterstained with DAPI (red). Values for percentage nuclear phosphorylated p53^{Ser15} and apoptotic cells are indicated and highlighted by a black border in A. Scale bar, 20 μ m. D, RT-PCR analysis of *Cdkn1a* expression relative to *Actb*. *Cdkn1a* expression was evaluated in Th-MYCNI/Trp53^{WT/WT} untreated tumors ($n = 5$) or tumors treated with IR ($n = 6$), as well as Th-MYCNI/Trp53^{KI/KI} untreated tumors ($n = 5$) or tumors treated with IR minus tamoxifen (Tam; $n = 5$) or plus tamoxifen ($n = 4$). *, $P = 0.04$; ****, $P < 0.0001$; unpaired t test. E, correlation plot between the intratumoral concentrations of 4-OHT and tamoxifen expressed in nmol/L (left, $r = 0.86$, $n = 8$, $P < 0.01$) and correlation plot between intratumoral concentrations of 4-OHT and percentage of dead cells (right, $r = 0.01$, $n = 8$, $P = 0.97$).

**Figure 3.**

Transcriptomic analysis of p53-deficient tumors reveals upregulation of GSH antioxidant pathway genes and an increased GSH pool and purine metabolism. A–D, Affymetrix mouse transcriptome array analysis of Th-MYCN/Trp53^{WT/WT} (n = 4) and Th-MYCN/Trp53^{KI/KI} (n = 8) tumors. A, hierarchical clustering. B, principal component analysis of signal intensities. C, overall survival of human neuroblastoma patients according to low or high expression of GSTP1 and GSTZ1 (<http://r2.amc.nl>, Versteeg-88 database of human neuroblastoma samples, GEO Series GSE16476). D, schematic representation of the glutathione metabolic pathway. E, analysis of GSH using the GSH-Glo glutathione assay in samples from MYCN/Trp53^{WT/WT} tumors (n = 4), untreated Th-MYCN/Trp53^{KI/KI} tumors (n = 6), or Th-MYCN/Trp53^{KI/KI} tumors treated with tamoxifen (n = 4). *, P = 0.02; unpaired t test. Error bars, mean ± SD. ns, nonsignificant.

we identified the glutathione metabolism pathway, which is associated with drug resistance (21–23), to be differentially regulated (Supplementary Table S3). An examination of genes encoding components of the glutathione metabolism pathway in individual tumors revealed upregulation in 50% of Th-MYCN/Trp53^{KI/KI} tumors. Furthermore, the glutathione S-transferase (GST) family, including *Gstz1* and *Gstp1*, represented the largest group (7 of 17 genes; Table 1). Glutathione and antioxidants have been shown to affect tumor initiation and drug resistance (23) and overexpression of *GSTP1* (24) and *GSTZ1* correlate with poor survival in neuroblastoma patients (Fig. 3C).

p53 deficiency leads to an increase in the GSH pool in response to chronic oxidative stress in MYCN-driven neuroblastoma

GST catalyzes the conjugation of the reduced form of glutathione (GSH) to xenobiotic substrates or unstable molecules such as hydrogen peroxide or other ROS for the purpose of detoxification (Fig. 3D). To examine whether the upregulation of GST is correlated with changes in the GSH redox cycle, we performed metabolic analysis using GC-MS. We identified 12 metabolites that were significantly altered between Th-MYCN/Trp53^{WT/WT} and Th-MYCN/Trp53^{KI/KI} tumors (Table 2). Consistent with our gene expression data, the glutathione pool was increased by 3.7-fold in Th-MYCN/Trp53^{KI/KI} tumors, together with a 4.3-fold decrease in

Table 1. Altered expression of genes in the glutathione pathway among individual Th-MYCN/Trp53^{KI/KI} tumors versus Th-MYCN/Trp53^{WT/WT} tumors

Gene	Sample					
	82078	83997	84834	28914	69306	72224 26857
<i>Gstm1</i>	+					+
<i>Gstm7</i>	+					+
<i>Gstm2</i>						+
<i>Gstm4</i>	+					
<i>Gstp1</i>				+		+
<i>Gstt1</i>					+	+
<i>Gstz</i>						+
<i>Mgst3</i>	+					
<i>Gstm3</i>	+					+
<i>Rrm2</i>				+		+
<i>Anpep</i>						
<i>Gclc</i>	+					
<i>Gpx3</i>	+			+		+
<i>Gstt2</i>						+
<i>Gstk1</i>						+
<i>Mgst1</i>						+
<i>Mgsta3</i>						+

NOTE: +, altered expression of genes among individual Th-MYCN/Trp53^{KI/KI}.

glycine, a glutathione precursor (Table 2). The increase in GSH in Th-MYCN/Trp53^{KI/KI} tumors was confirmed using the GSH-Glo glutathione assay (Fig. 3E). Interestingly, p53 restoration did not reverse this metabolic adaptation, with high GSH levels maintained in Th-MYCN/Trp53^{KI/KI} tumors. Upregulation of the GSH antioxidant metabolic pathway in p53-deficient MYCN-driven neuroblastoma suggested an increased requirement for detoxification of GST substrates, such as derivatives of ROS that are implicated in tumorigenesis, disease progression, and drug-induced resistance (25). Furthermore, c-MYC overexpression and p53 loss of function have previously been shown to be associated with an alteration in ROS levels (2, 26–28). Consistent with these results, we found a significant increase in ROS-positive cells in Th-MYCN/Trp53^{KI/KI} tumors (mean of 64%) compared with Th-MYCN/Trp53^{WT/WT} tumors (mean of 14%; Fig. 4A–C). Furthermore, in agreement with the data shown in Fig. 2, restoration of p53ER^{TAM} activity reduced the percentage of ROS-positive cells in approximately 50% of tumors (Fig. 4C). This suggests that enhanced ROS levels may be regulated (either directly or indirectly) by p53 in a fraction of Th-MYCN/Trp53^{KI/KI} tumors. As noted above, this was not associated with a decrease in tumor growth or improved overall survival (Supplementary Fig. S3). Evidence for the presence of increased oxidative stress in Th-MYCN/Trp53^{KI/KI} tumors was supported by the finding of enhanced staining for 8-hydroxyguanosine (8-OHdG), a modified base that occurs in DNA due to attack by hydroxyl radicals (Fig. 4D; ref. 29). ROS levels can also be increased by hypoxia and staining with the hypoxia marker pimonidazole, which revealed that Th-MYCN/Trp53^{KI/KI} tumors contained increased perinecrotic hypoxic regions (Fig. 4E and F). Increased ROS has been reported to lead to damage to enzymes, membranes, and DNA (29, 30), but despite enhanced 8-OHdG staining (Fig. 4D), we found no significant changes in the levels of DNA damage markers (p-CHEK2 and γ -H2AX) between untreated Th-MYCN/Trp53^{WT/WT} and Th-MYCN/Trp53^{KI/KI} tumors (Supplementary Fig. S5).

Our results suggest that resistance to IR in Th-MYCN/Trp53^{KI/KI} mice may be due to metabolic adaption to chronic oxidative stress through upregulation of GST pathway genes and increased levels of antioxidant metabolites. This implied that the depletion of the GSH pool could resensitize IR-resistant

p53-deficient neuroblastoma cells. Thus, we treated tumors with buthionine sulfoximine (BSO), an inhibitor of GSH synthesis that targets glutamate cysteine ligase (GCL), the first enzyme of the cellular GSH biosynthetic pathway (Fig. 3D). We implanted Th-MYCN/Trp53^{KI/KI} primary tumor cells subcutaneously into 129 \times 1/SvJ-Tg Th-MYCN-negative mice. Consistent with our findings in the Th-MYCN/Trp53^{KI/KI} GEM model of spontaneous neuroblastoma, 50% of the allografted tumors in which p53 activity was restored by the addition of Tam displayed resistance to 5 Gy IR and a higher Ki-67 proliferative index (Fig. 5A). However, importantly, this resistance was abolished in the presence of BSO (250 mg/kg; Fig. 5B and C).

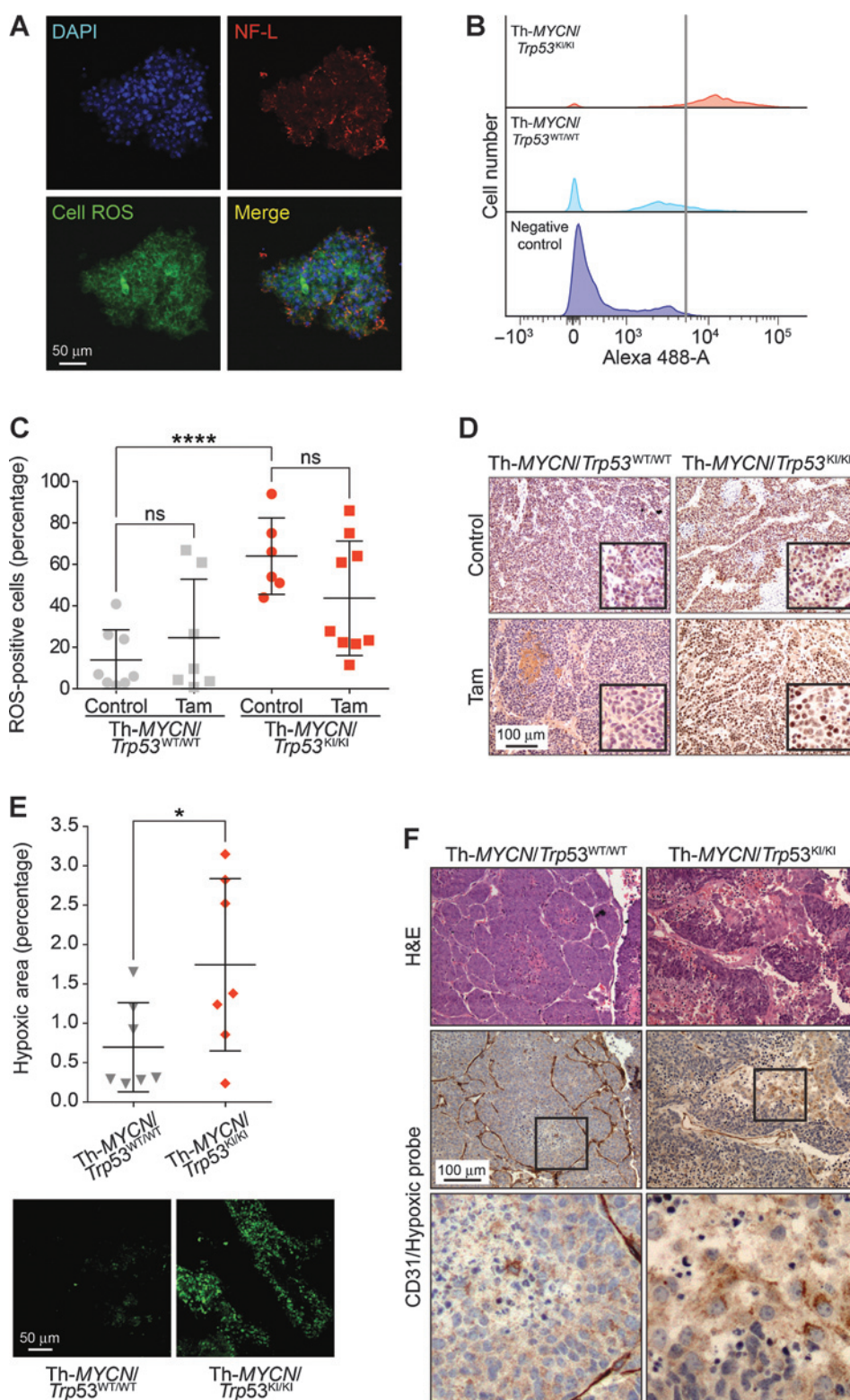
Discussion

In this study, we have demonstrated that p53 deficiency combines with aberrant expression of MYCN to drive neuroblast hyperplasia and increased neuroblastoma penetrance. Restoration of functional p53ER^{TAM} prior to tumors reaching detectable size or during later stages failed to alter tumor growth or penetrance. These findings suggest that p53 has an important role in the early stages of neuroblastoma tumorigenesis in Th-MYCN transgenic mice. Furthermore, p53 loss of function gives rise to tumors that can acquire growth and survival mechanisms that are resistant to the reintroduction of functional p53. This is in stark contrast with a medulloblastoma GEM model driven by expression of MYCN and p53 deficiency, GTML/Trp53^{KI/KI} (GTML; *Glt1-tTA/TRE-MYCN-Luc*), where restoration of functional p53ER^{TAM} by Tam led to increased survival and inhibition of tumor growth (5). Other transgenic models of p53 loss of function do, however, develop tumors that display partial resistance to the restoration of functional p53ER^{TAM} including lymphoma where a requirement for induction of the oncogenic signaling sensor p19^{ARF} was identified (31). In addition, p53 restoration in K-Ras-induced non-small cell lung cancer failed to induce tumor regression, but diminished the proportion of high-grade tumors (32).

Recent results have suggested that the outcome of p53 restoration in established tumors is highly context-dependent. There is now evidence that the tumor suppressor function of p53 may be due to maintenance of genomic stability as well as metabolic and oxidative balance rather than simply its canonical role as a transcriptional activator of cell-cycle inhibitory and proapoptotic effectors, such as p21, PUMA, and NOXA (1, 3). Consistent with these findings, we found that tumors with p53 loss of function displayed elevated ROS. Three characteristics of Th-MYCN/Trp53^{KI/KI} tumors could contribute to the increased levels of ROS: MYCN expression, hypoxia, and p53 loss of function.

Table 2. Analysis of metabolites in p53-deficient tumors

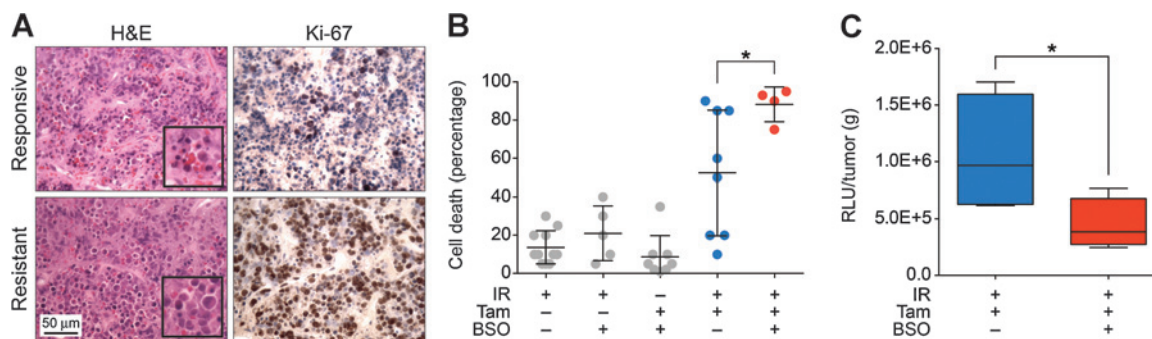
Metabolite	KIKI:WT/WT Ratio	P value
Alanine	0.480	1.23E–02
Valine	0.496	3.26E–02
Threonine	0.544	3.90E–02
Glycine	0.233	2.38E–02
Succinate	0.631	4.47E–02
PEP	0.538	3.52E–02
Hypotaurine	0.382	4.50E–02
Hypoxanthine	1.924	2.81E–02
3-GP	0.531	4.33E–02
L-ascorbic acid	0.397	3.18E–02
Ribose-5-phosphate	0.651	3.13E–02
GSH pool	3.761	1.66E–02

**Figure 4.**

Th-MYCNI/Trp53^{K1/K1} tumors exhibit chronic oxidative stress. A, fluorescence staining for NF-L expression and the presence of ROS in Th-MYCNI/Trp53^{K1/K1} tumor cells. Scale bar, 50 μ m. B, histogram of ROS intensity as stained by CellROX Green in Th-MYCNI/Trp53^{K1/K1}, Th-MYCNI/Trp53^{WT/WT}, or unstained negative control cells as indicated. Gray bar represents the intensity threshold for ROS positivity. C, flow cytometric analysis of ROS-positive cells in Th-MYCNI/Trp53^{WT/WT} tumors with ($n = 7$) or without ($n = 9$) tamoxifen or Th-MYCNI/Trp53^{K1/K1} tumors with ($n = 6$) or without ($n = 4$) tamoxifen. ****, $P < 0.0001$; unpaired t test. D, staining for the oxidative stress marker 8-OHdG in Th-MYCNI/Trp53^{K1/K1} tumors. Scale bar, 100 μ m. E, top, fluorescence measurement of pimonidazole adduct formation in tumors from Th-MYCNI/Trp53^{WT/WT} ($n = 7$) or Th-MYCNI/Trp53^{K1/K1} ($n = 7$) mice. Data points represent the mean area for each individual tumor. *, $P = 0.04$; unpaired t test. Bottom, representative fluorescence images from Th-MYCNI/Trp53^{WT/WT} and Th-MYCNI/Trp53^{K1/K1} tumors as indicated. F, H&E and immunohistochemical costaining with CD31 and Hypoxprobe in Th-MYCNI/Trp53^{WT/WT} and Th-MYCNI/Trp53^{K1/K1} tumors. Scale bar, 100 μ m. Error bars represent mean \pm SD. Tam, tamoxifen; ns, nonsignificant.

MYCN-dependent metabolic adaptation has been shown to result in upregulation of glycolytic metabolism, which is associated with increase in ROS production (7, 33). Hypoxia, on the other hand, can generate ROS via mitochondrial complex III (34), and p53 has

been shown to regulate ROS and, in turn, to be regulated by ROS in a context-dependent manner (35). The low level of ROS in Th-MYCNI/Trp53^{WT/WT} compared with Th-MYCNI/Trp53^{K1/K1} tumors suggests that MYCN alone cannot be the only driver and that loss

**Figure 5.**

Depletion of the GSH pool restores sensitivity to IR. A–C, mice bearing allografts derived from Th-MYC/Trp53^{KI/KI} tumors were untreated ($n = 4$), treated with 5 Gy IR ($n = 4$), tamoxifen (Tam; $n = 4$), or 250 mg/kg BSO ($n = 4$). Mice were injected bilaterally with tumor cells, and six to eight tumors were analyzed per group. Scale bar, 50 μ m. A, H&E and immunohistochemical staining for cell proliferation (Ki-67) in Th-MYC/Trp53^{KI/KI} allografts responsive or resistant to treatment with IR and tamoxifen as indicated. B, quantitative histopathologic determination of cell death in Th-MYC/Trp53^{KI/KI} allografts treated with IR, tamoxifen, and/or BSO as indicated. C, total GSH levels in Th-MYC/Trp53^{KI/KI} allografts treated with IR and tamoxifen, with or without BSO as indicated. *, $P = 0.03$, unpaired t test (one-tailed). Error bars, mean \pm SD.

of p53 is also required. A number of direct p53 targets involved in the antioxidant pathway have been identified such as MnSOD, sestrins (Sesn1-3), NRF2, ALDH4 (aldehyde dehydrogenase 4), GLS2 (glutaminase 2), TIGAR, and tumor protein p53-inducible nuclear protein 1 (TP53INP1; refs. 2, 36). However, p53 also has a context-dependent pro-oxidant function and can transcriptionally upregulate genes with strong pro-oxidant properties, including PIG1–13 (p53-inducible genes 1–13; ref. 37). The dual pro-oxidant and antioxidant roles of p53 suggest a delicate interplay between p53 and ROS in normal cells, and in the absence of p53, one might expect to see the changes in the ROS-redox equilibrium identified in this study. Thus, the combination of MYCN expression, p53 loss of function, and hypoxia leading to elevated ROS in Th-MYC/Trp53^{KI/KI} tumors may account for the resistance to cell death in the absence of functional p53^{ER^{TAM}}. However, the lack of cell death upon restoration of functional p53^{ER^{TAM}} indicates that other mechanisms arose to compensate for the increased oxidative stress.

There are several reducing mechanisms that regulate ROS-driven oxidative stress by transferring an unstable electron to a stable molecule. Among them is the glutathione pathway, where glutathione peroxidase reduces hydrogen peroxide to water, while it oxidizes GSH to form dithiol (GSSH). Several genes from the GSH pathway are regulated by p53, which can down-regulate glutathione peroxidase 1 (GPX1) and glutaredoxin 3 (GRX3) to reduce ROS (38, 39). A compensatory increase in the GSH pathway in the absence of functional p53 is supported by our results with Th-MYC/Trp53^{KI/KI} tumors exhibiting significant changes in the glutathione pathway, further confirmed by an increase in the GSH pool as measured by multiple assays. In addition to the direct detoxification of hydrogen peroxide by GSH, GSH can also be conjugated to xenobiotic substrates for the purpose of detoxification of the metabolites produced within the cell by oxidative stress. This reaction is catalyzed by GST. Interestingly, we found that 7 of 12 of the altered genes in glutathione metabolism pathway are from the GST family. Upregulation of GSTs is associated with chemoresistance and appears to represent an adaptive response to increased cellular damage and an important protective mechanism (33, 35, 40). This role of GST is consistent with the resistance to IR exhibited

by Th-MYC/Trp53^{KI/KI} tumors, even after restoration of functional p53^{ER^{TAM}}. *GSTP1* is transcriptionally regulated by MYCN (24) and, alongside *GSTZ1*, high expression of these genes is linked with poor outcome in neuroblastoma (<http://r2.amc.nl>). Consistent with this, high levels of GSH are associated with resistance to chemotherapeutic and targeted therapies, including those used in frontline treatment of neuroblastoma, such as cyclophosphamide, as well as relapsed disease, such as irinotecan and temozolomide (41–44).

The continuing high relapse rate and poor survival for high-risk neuroblastoma patients make the development of new therapeutic approaches an urgent priority. While direct mutations to p53 are a rare event in *de novo* cases of neuroblastoma (6), examination of the p53 pathway has underlined its role in the pathogenesis of high-risk neuroblastoma (45–50). The role of p53 loss of function in the pathogenesis of untreated neuroblastomas has thus far not been elucidated. Our study, however, strongly suggests that p53 plays an important role in the maintenance of redox homeostasis. Thus, in the absence of p53, tumors may metabolically adapt to acquire prosurvival characteristics that nullify the canonical proapoptotic effects of p53. We therefore suggest that strategies to target neuroblastomas with defective p53 function using reactivation of p53 through inhibition of the MDM2/p53 interaction would not be successful in a proportion of cases. Here, pharmacologic depletion of the GSH pool together with reactivation of p53 represents an alternative strategy. Furthermore, high GSH pool levels or elevated expression of *GSTP1*, *GSTZ1*, or other glutathione pathway genes could serve as biomarkers for the stratification patients. In this study, we used BSO, an inhibitor of GCL, to deplete the GSH pool, but specific inhibitors of *GSTP1* such as 8-methoxypsoralen are currently under development (51). The use of agents to deplete the GSH pool in combination with conventional therapeutics or molecularly targeted drugs thus warrants further study in high-risk neuroblastoma.

Disclosure of Potential Conflicts of Interest

No potential conflicts of interest were disclosed.

Yogev et al.

Authors' Contributions

Conception and design: O. Yogev, L. Chesler

Development of methodology: O. Yogev, A. Hallsworth, Y. Jamin, R. Ruddle, F.I. Raynaud, L. Chesler

Acquisition of data (provided animals, acquired and managed patients, provided facilities, etc.): O. Yogev, K. Barker, A. Sikka, G.S. Almeida, A. Hallsworth, L.M. Smith, Y. Jamin, R. Ruddle, A. Koers, H.T. Webber, F.I. Raynaud, H.C. Keun, L. Chesler

Analysis and interpretation of data (e.g., statistical analysis, biostatistics, computational analysis): O. Yogev, A. Sikka, G.S. Almeida, Y. Jamin, R. Ruddle, S. Popov, C. Jones, K. Petrie, S.P. Robinson, H.C. Keun, L. Chesler

Writing, review, and/or revision of the manuscript: O. Yogev, K. Barker, G.S. Almeida, A. Hallsworth, Y. Jamin, F.I. Raynaud, K. Petrie, S.P. Robinson, H.C. Keun, L. Chesler

Administrative, technical, or material support (i.e., reporting or organizing data, constructing databases): O. Yogev, K. Barker, A. Hallsworth, L.M. Smith, L. Chesler

Study supervision: S.P. Robinson, L. Chesler

Acknowledgments

The authors thank Alan Mackay, Pawan Poudel, and Anguraj Sadanandam for valuable advice on bioinformatic analysis; Elizabeth Want and

Volker Behrends for advice on mass-spectrometry analysis. They also thank Sue Eccles and Eitan Shaulian for critical reading of the article.

Grant Support

This study was supported by grants from The Neuroblastoma Society (O. Yogev and K. Barker), MRC funding (MR/J015938/1 to A. Sikka), The Felix White Cancer Charity (A. Hallsworth), Cancer Research UK and EPSRC to the Cancer Imaging Centre at the Institute of Cancer Research (ICR) and The Royal Marsden Hospital, in association with the MRC and Department of Health (England; C1060/A10334 and C1060/A16464), The Wellcome Trust (091763Z/10/Z), an EPSRC Platform Grant (EP/H046526/1), NHS funding to the NIHR Biomedical Research Centre at The Royal Marsden and the ICR, and a Paul O'Gorman Postdoctoral Fellowship funded by Children with Cancer UK (Y. Jamin).

The costs of publication of this article were defrayed in part by the payment of page charges. This article must therefore be hereby marked *advertisement* in accordance with 18 U.S.C. Section 1734 solely to indicate this fact.

Received July 20, 2015; revised December 31, 2015; accepted February 9, 2016; published OnlineFirst March 29, 2016.

References

- Valente LJ, Gray DH, Michalak EM, Pinon-Hofbauer J, Egle A, Scott CL, et al. p53 efficiently suppresses tumor development in the complete absence of its cell-cycle inhibitory and proapoptotic effectors p21, Puma, and Noxa. *Cell Rep* 2013;3:1339–45.
- Puzio-Kuter AM. The role of p53 in metabolic regulation. *Genes Cancer* 2011;2:385–91.
- Vousden KH, Ryan KM. p53 and metabolism. *Nat Rev Cancer* 2009;9:691–700.
- Berkers CR, Maddocks OD, Cheung EC, Mor I, Vousden KH. Metabolic regulation by p53 family members. *Cell Metab* 2013;18:617–33.
- Hill RM, Kuijper S, Lindsey JC, Petrie K, Schwalbe EC, Barker K, et al. Combined MYC and P53 defects emerge at medulloblastoma relapse and define rapidly progressive, therapeutically targetable disease. *Cancer Cell* 2015;27:72–84.
- Pugh TJ, Morozova O, Attiye EF, Asgharzadeh S, Wei JS, Auclair D, et al. The genetic landscape of high-risk neuroblastoma. *Nat Genet* 2013;45:279–84.
- Qing G, Li B, Vu A, Skuli N, Walton ZE, Liu X, et al. ATF4 regulates MYC-mediated neuroblastoma cell death upon glutamine deprivation. *Cancer Cell* 2012;22:631–44.
- Rapizzi E, Ercolino T, Fucci R, Zampetti B, Felici R, Guasti D, et al. Succinate dehydrogenase subunit B mutations modify human neuroblastoma cell metabolism and proliferation. *Horm Cancer* 2014;5:174–84.
- Das S, Bryan K, Buckley PG, Piskareva O, Bray IM, Foley N, et al. Modulation of neuroblastoma disease pathogenesis by an extensive network of epigenetically regulated microRNAs. *Oncogene* 2013;32:2927–36.
- Wang C, Liu Z, Woo CW, Li Z, Wang L, Wei JS, et al. EZH2 Mediates epigenetic silencing of neuroblastoma suppressor genes CASZ1, CLU, RUNX3, and NGFR. *Cancer Res* 2012;72:315–24.
- Fukuoka H, Takahashi Y. The role of genetic and epigenetic changes in pituitary tumorigenesis. *Neurol Med Chir* 2014;54:943–57.
- Workman P, Aboagye EO, Balkwill F, Balmain A, Bruder G, Chaplin DJ, et al. Guidelines for the welfare and use of animals in cancer research. *Br J Cancer* 2010;102:1555–77.
- Kilkenny C, Browne WJ, Cuthill IC, Emerson M, Altman DG. Improving bioscience research reporting: The ARRIVE guidelines for reporting animal research. *PLoS Biol* 2010;8:e1000412.
- Weiss WA, Aldape K, Mohapatra G, Feuerstein BG, Bishop JM. Targeted expression of MYCN causes neuroblastoma in transgenic mice. *EMBO J* 1997;16:2985–95.
- Christophorou MA, Martin-Zanca D, Soucek L, Lawlor ER, Brown-Swigart L, Verschuren EW, et al. Temporal dissection of p53 function in vitro and in vivo. *Nat Genet* 2005;37:718–26.
- Jamin Y, Tucker ER, Poon E, Popov S, Vaughan L, Boulton JK, et al. Evaluation of clinically translatable MR imaging biomarkers of therapeutic response in the TH-MYC transgenic mouse model of neuroblastoma. *Radiology* 2013;266:130–40.
- Boulton JK, Walker-Samuel S, Jamin Y, Leiper JM, Whitley GS, Robinson SP. Active site mutant dimethylarginine dimethylaminohydrolase 1 expression confers an intermediate tumour phenotype in C6 gliomas. *J Pathol* 2011;225:344–52.
- Rasmuson A, Segerstrom L, Nethander M, Finnman J, Elfman LH, Javanmardi N, et al. Tumor development, growth characteristics and spectrum of genetic aberrations in the TH-MYC transgenic mouse model of neuroblastoma. *PLoS One* 2012;7:e51297.
- Hansford LM, Thomas WD, Keating JM, Burkhardt CA, Peaston AE, Norris MD, et al. Mechanisms of embryonal tumor initiation: distinct roles for MycN expression and MYCN amplification. *Proc Natl Acad Sci U S A* 2004;101:12664–9.
- Matthay KK, Villablanca JG, Seeger RC, Stram DO, Harris RE, Ramsay NK, et al. Treatment of high-risk neuroblastoma with intensive chemotherapy, radiotherapy, autologous bone marrow transplantation, and 13-cis-retinoic acid. Children's Cancer Group. *N Engl J Med* 1999;341:1165–73.
- Townsend DM, Tew KD. The role of glutathione-S-transferase in anticancer drug resistance. *Oncogene* 2003;22:7369–75.
- Tew KD. Glutathione-associated enzymes in anticancer drug resistance. *Cancer Res* 1994;54:4313–20.
- Traverso N, Ricciarelli R, Nitti M, Marengo B, Furfaro AL, Pronzato MA, et al. Role of glutathione in cancer progression and chemoresistance. *Oxid Med Cell Longev* 2013;2013:972913.
- Fletcher JI, Gherardi S, Murray J, Burkhardt CA, Russell A, Valli E, et al. N-Myc regulates expression of the detoxifying enzyme glutathione transferase GSTP1, a marker of poor outcome in neuroblastoma. *Cancer Res* 2012;72:845–53.
- Sosa V, Moline T, Somoza R, Paciucci R, Kondoh H, Meli LL. Oxidative stress and cancer: An overview. *Ageing Res Rev* 2013;12:376–90.
- Graves JA, Metukuri M, Scott D, Rothermund K, Prochownik EV. Regulation of reactive oxygen species homeostasis by peroxiredoxins and c-Myc. *J Biol Chem* 2009;284:6520–9.
- Ostrakhovitch EA, Cherian MG. Role of p53 and reactive oxygen species in apoptotic response to copper and zinc in epithelial breast cancer cells. *Apoptosis* 2005;10:111–21.
- Vafa O, Wade M, Kern S, Beeche M, Pandita TK, Hampton GM, et al. c-Myc can induce DNA damage, increase reactive oxygen species, and mitigate p53 function: a mechanism for oncogene-induced genetic instability. *Mol Cell* 2002;9:1031–44.

29. Ziech D, Franco R, Pappa A, Panayiotidis MI. Reactive oxygen species (ROS)-induced genetic and epigenetic alterations in human carcinogenesis. *Mutat Res* 2011;711:167–73.
30. Cooke MS, Evans MD, Dizdaroglu M, Lunec J. Oxidative DNA damage: Mechanisms, mutation, and disease. *FASEB J* 2003;17:1195–214.
31. Martins CP, Brown-Swigart L, Evan GI. Modeling the therapeutic efficacy of p53 restoration in tumors. *Cell* 2006;127:1323–34.
32. Junttila MR, Karnezis AN, Garcia D, Madriles F, Kortlever RM, Rostker F, et al. Selective activation of p53-mediated tumour suppression in high-grade tumours. *Nature* 2010;468:567–71.
33. Sabharwal SS, Schumacker PT. Mitochondrial ROS in cancer: Initiators, amplifiers or an Achilles' heel? *Nat Rev Cancer* 2014;14:709–21.
34. Guzy RD, Hoyos B, Robin E, Chen H, Liu L, Mansfield KD, et al. Mitochondrial complex III is required for hypoxia-induced ROS production and cellular oxygen sensing. *Cell Metab* 2005;1:401–8.
35. Maillet A, Pervaiz S. Redox regulation of p53, redox effectors regulated by p53: A subtle balance. *Antioxid Redox Signal* 2012;16:1285–94.
36. Budanov AV. The role of tumor suppressor p53 in the antioxidant defense and metabolism. *Subcell Biochem* 2014;85:337–58.
37. Polyak K, Xia Y, Zweier JL, Kinzler KW, Vogelstein B. A model for p53-induced apoptosis. *Nature* 1997;389:300–5.
38. Brynczka C, Labhart P, Merrick BA. NGF-mediated transcriptional targets of p53 in PC12 neuronal differentiation. *BMC Genomics* 2007;8:139.
39. Tan M, Li S, Swaroop M, Guan K, Oberley LW, Sun Y. Transcriptional activation of the human glutathione peroxidase promoter by p53. *J Biol Chem* 1999;274:12061–6.
40. Waypa GB, Marks JD, Guzy R, Mungai PT, Schriewer J, Dokic D, et al. Hypoxia triggers subcellular compartmental redox signaling in vascular smooth muscle cells. *Circ Res* 2010;106:526–35.
41. Rocha CR, Garcia CC, Vieira DB, Quinet A, de Andrade-Lima LC, Munford V, et al. Glutathione depletion sensitizes cisplatin- and temozolomide-resistant glioma cells in vitro and in vivo. *Cell Death Dis* 2015;6:e1727.
42. Estrela JM, Ortega A, Obrador E. Glutathione in cancer biology and therapy. *Crit Rev Clin Lab Sci* 2006;43:143–81.
43. Montero AJ, Jassem J. Cellular redox pathways as a therapeutic target in the treatment of cancer. *Drugs* 2011;71:1385–96.
44. St-Coeur PD, Poitras JJ, Cuperlovic-Culf M, Touaibia M, Morin PJ. Investigating a signature of temozolomide resistance in GBM cell lines using metabolomics. *J Neurooncol* 2015;125:91–102.
45. Tweddle DA, Pearson AD, Haber M, Norris MD, Xue C, Flemming C, et al. The p53 pathway and its inactivation in neuroblastoma. *Cancer Lett* 2003;197:93–8.
46. Tweddle DA, Malcolm AJ, Cole M, Pearson AD, Lunec J. p53 cellular localization and function in neuroblastoma: Evidence for defective G(1) arrest despite WAF1 induction in MYCN-amplified cells. *Am J Pathol* 2001;158:2067–77.
47. Kim E, Shohet J. Targeted molecular therapy for neuroblastoma: The ARF/MDM2/p53 axis. *J Natl Cancer Inst* 2009;101:1527–9.
48. Wolff A, Technau A, Ihling C, Technau-Ihling K, Erber R, Bosch FX, et al. Evidence that wild-type p53 in neuroblastoma cells is in a conformation refractory to integration into the transcriptional complex. *Oncogene* 2001;20:1307–17.
49. Gamble LD, Kees UR, Tweddle DA, Lunec J. MYCN sensitizes neuroblastoma to the MDM2-p53 antagonists Nutlin-3 and MI-63. *Oncogene* 2012;31:752–63.
50. Xue C, Haber M, Flemming C, Marshall GM, Lock RB, MacKenzie KL, et al. p53 determines multidrug sensitivity of childhood neuroblastoma. *Cancer Res* 2007;67:10351–60.
51. de Oliveira DM, de Farias MT, Teles AL, Dos Santos Junior MC, de Cerqueira MD, Lima RM, et al. 8-Methoxypsoralen is a competitive inhibitor of glutathione S-transferase P1-1. *Front Cell Neurosci* 2014;8:308.

Cancer Research

The Journal of Cancer Research (1916–1930) | The American Journal of Cancer (1931–1940)

p53 Loss in MYC-Driven Neuroblastoma Leads to Metabolic Adaptations Supporting Radioresistance

Orli Yogev, Karen Barker, Arti Sikka, et al.

Cancer Res 2016;76:3025-3035. Published OnlineFirst March 29, 2016.

Updated version	Access the most recent version of this article at: doi: 10.1158/0008-5472.CAN-15-1939
Supplementary Material	Access the most recent supplemental material at: http://cancerres.aacrjournals.org/content/suppl/2017/02/06/0008-5472.CAN-15-1939.DC2

Cited articles	This article cites 51 articles, 9 of which you can access for free at: http://cancerres.aacrjournals.org/content/76/10/3025.full#ref-list-1
-----------------------	---

E-mail alerts	Sign up to receive free email-alerts related to this article or journal.
Reprints and Subscriptions	To order reprints of this article or to subscribe to the journal, contact the AACR Publications Department at pubs@aacr.org .
Permissions	To request permission to re-use all or part of this article, use this link http://cancerres.aacrjournals.org/content/76/10/3025 . Click on "Request Permissions" which will take you to the Copyright Clearance Center's (CCC) Rightslink site.